

MULTI-DISCIPLINARY OPTIMIZATION INCLUDING ENVIRONMENTAL ASPECTS APPLIED TO SUPERSONIC AIRCRAFT

J. Brezillon*, G. Carrier **, M. Laban***

*** German Aerospace Centre (DLR), Braunschweig, Germany,**

**** The French Aerospace Lab (ONERA), Meudon, France,**

***** National Aerospace Laboratory (NLR), Amsterdam, the Netherlands**

Keywords: *multi-disciplinary optimization, supersonic, CFD, CSM, sonic boom*

Abstract

The paper presents the multi-disciplinary optimization framework developed by the authors and applied to the optimization of small size supersonic aircraft. This framework, based on the combination of low(empirical model) and high fidelity (CFD, CSM) tools to simulate the complete mission of the aircraft, allows the investigation of the trade-off that exists between the aircraft performance (maximum take-off weight, mission range) and the sonic-boom overpressure, one of the more severe environmental constraints for supersonic aircraft.

1 Introduction

In the current corporate world, where companies are spread across several continents and where business is conducted all around the globe, the required time for travel has become a valuable resource, prompting interest in high-speed transportation. Compared to a classical flight at Mach $M=0.8$ with a mission range of 4000 Nautical miles (nm), up to a 55% time savings can be achieved by increasing the cruise speed up to $M=1.8$ [1].

However, a successful supersonic aircraft design has to overcome numerous challenges to meet opposing requirements such as a highly efficient aerodynamic wing both at high- and low-speeds, light structural weight to sustain high loads at high speed, small by-pass ratio engine and low fuel consumption, high speed and low ticket price. Furthermore,

environmental constraints become more and more stringent - low perceived noise level and emissions at landing and take-off, low emissions at high altitude and a minimum level of sonic boom overpressures at supersonic flight - making the viability of supersonic aircraft extremely difficult.

Many studies over the last decades were conducted in the US, Europe and Japan to develop solutions for these challenging problems. It is now agreed that small-size supersonic transport aircraft are likely to be the next supersonic aircraft on the market. The business jets have indeed the major advantages 1) to be relatively small and lightweight which is beneficial for sonic boom annoyance level, 2) to rely on "conventional" commercial core engines 3) to have a market segment where the additional cost for supersonic travel has limited impact. However a small size supersonic aircraft has specific difficulties like a lower aerodynamic efficiency due to a larger fuselage relative size and a smaller volume for fuel. In consequence, the design of new supersonic aircraft will need dedicated design processes capable to take into account all these conflicting requirements to end up with a good overall design.

Within earlier projects, DLR, NLR and Onera have accumulated significant experience and have now in hand a common multi-disciplinary analysis suite (MDA) dedicated to supersonic aircraft applications [2-4]. This procedure, originally developed by NLR and later adapted to the DLR and Onera tools, is relying on high fidelity disciplines for

aerodynamics and structure (in supersonic cruise) and on statistics-based tools to cover other disciplines (flight mechanics and propulsion) and the remaining parts of the mission.

In the European project HiSAC [5] ("environmentally friendly High Speed Aircraft"), the above mentioned multi-disciplinary suite was adapted and successfully applied to small-size supersonic transport aircraft [6, 7]. Later, Onera extended the multi-disciplinary suite by implementing a sonic boom overpressure module which propagates the pressure disturbances introduced by the aircraft in its near field through the atmosphere down to the ground. The resulting suite permits the prediction of the overall aircraft characteristics, from the technical performance up to the environmental aspects.

The paper first presents the supersonic aircraft concepts and the main characteristics of the multi-disciplinary suite and finally gives some insight into optimal configurations.

2 Initial configurations

Within the HiSAC project, a set of top-level requirements were established for a supersonic business-jet carrying 8 passengers. In the present study, 2 aircraft concepts following different strategies are explored in detail.

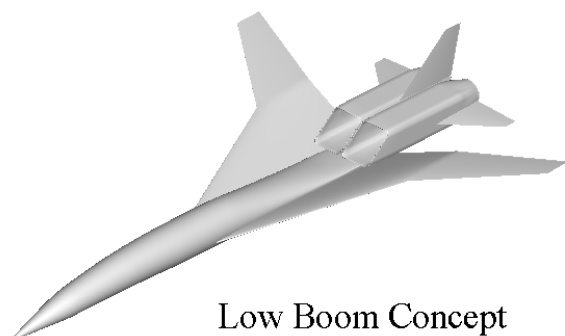


Fig. 1. Shape of the Low Boom Concept

The first configuration, developed by the Russian design team (Sukhoy, Tsagi, Ciamp), is a low-boom concept with a cruise Mach number of $M=1.8$ and an initial start of cruise altitude of 53,000 feet. It is characterised by a double delta wing with significant dihedral for sonic boom mitigation, as presented in Fig. 1. The

configuration features two engines mounted side-by-side on top of the rear part of the fuselage. The latter was designed to allow air into the engine intakes and to provide area ruling.

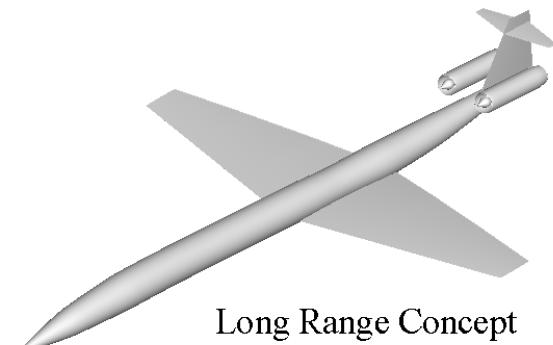


Fig. 2. Shape of the Long Range Concept

The second concept, explored by the Italian design team (Alenia), relies essentially on extensive zones of laminar flow to obtain lower drag and thus a higher aerodynamic efficiency. In consequence, less thrust will be required and should allow for a smaller engine and less fuel consumption. The natural laminar wing is also potentially better than a classical delta wing in subsonic cruise and at low speed. Such a configuration, cruising at a Mach number of $M=1.6$ and 41,000 feet altitude, should be well suited to complete a long-range mission. The baseline shape presented in Fig. 2, is characterized by a single-trapezoidal wing with a low sweep angle, no dihedral and no leading-edge crank that would cause boundary layer transition to turbulent flow. Also to promote large areas of laminar flow, double-lens type airfoils are used for sustained chord-wise positive pressure gradients. During the HiSAC project, various engine and tail designs were presented by Alenia and for the present work, one of their earlier designs has been retained: it features two engines mounted on either side of the vertical T-tail at the rear of the fuselage

3 Mixed Fidelity MDO framework

3.1 The MDO Framework Architecture

A generic multi-disciplinary analysis and optimization framework for aeronautical

products was developed and matured at NLR during the last decade. Recent applications included the classical transonic transport aircraft [8, 9], the blended-wing body [10], and the supersonic transport aircraft [3]. The disciplines of aerodynamics and structural mechanics take a central place but various other contributing disciplines are also called in. During the HiSAC project, the MDA suite has been adapted for small-size supersonic transport aircraft and Onera developed a complementary environmental module dedicated to sonic boom overpressure prediction. The main components of the framework, configured for supersonic aircraft applications comprise:

1. A Geometry module providing the parametric external (aerodynamic) and internal (structural) shape of the configuration.
2. A Weight and Balance module keeping a record of all items contributing to the mass and centre of gravity of the configuration.
3. A Structural Optimization module sizing the structural element thicknesses to arrive at a minimum weight primary wing structure. The structural element sizing is based on a finite element (FE) analysis combined with analytical representations of details not covered by the FE representation.
4. An Aerodynamic Performance module analysing the aircraft lift over drag (L/D) performance. CFD-based methods are used for the cruise condition and dedicated empirical models, derived from conceptual design phase tools, permit to either estimate the viscous drag contribution in cruise or predict the aerodynamic performance at off-design flight phases.
5. An Engine Sizing module modelling the thermodynamic cycles of the engine for maximum propulsive efficiency and sizing the propulsion system to meet the aircraft thrust requirements.
6. A Flight Mechanics module assessing the aircraft take-off and landing performance as well as the static stability and the ability to trim the configuration.
7. A Mission Analysis module which collects the results from all contributing analysis disciplines and computes the aircraft mission range.

8. A Sonic Boom Overpressure module that propagates to the ground the shock waves and pressure disturbances generated by the aircraft in supersonic flight and gives figures of merit of the signature at ground.

An extensive description of the modules 1 to 7 for supersonic aircraft optimization applications can be found in [6]. Module 8 is explained in more detail in chapter 3.5 below.

The framework relies on mixed fidelity, as outlined in chapter 3.3 and 3.4, as well as on mixed-level approaches. At the global level, quantities such as maximum take-off weight (MTOW), mission range or sonic boom characteristics can be used by an optimizer to drive the overall design process. Dedicated design parameters - typically fuselage and wing parameters - are associated to this top level and have a direct impact on all disciplines. For every set of global-level parameters, local-level parameters are used for single disciplinary local-optimizations. These local-optimizations are in charge to end up with a minimal structural weight, low installed fuel consumption or optimal aircraft ascent and descent trajectories for minimum range loss.

The resulting framework was shared between NLR, Onera and DLR with identical processes for low fidelity models, but each partner uses his own high fidelity methods. The applications presented in the following chapters were achieved based on the process chain deployed at DLR. Compared to the MDA used in [7] some modules have been updated and adapted for the sonic boom signature and the global architecture has been tuned for simultaneous evaluations on large-scale computing clusters.

3.2 Parametrisation

The geometry generation module is responsible for defining the external (aerodynamic) and internal (structural) shape of the configuration. Although the scope of the investigation is mainly driven by wing planform/airfoil modifications, the complete aircraft geometry definition is still required to support global-level aircraft performance evaluations. The shapes of the tailplanes remain

fixed and are read in as a priori defined data files. The engine nacelle geometry is also predefined, but is then scaled to follow thrust requirements delivered by the engine sizing module.

The wing and (optionally) the fuselage geometry generation are set up in a parametric way for fast design space explorations. The wing planform, modelled as a double trapezoid, is described by the nine parameters presented in Fig. 3. For the low sonic boom concept, the inner- and outer-wing dihedrals are also set as design parameters. Additional parameters are used to define the thickness-to-chord ratio and the twist at specific wing sections, like (but not limited to) the root, crank and tip. All these parameters are directly driven by the global-level optimizer.

For the CFD, the geometry considered is limited to the fuselage and wing parts. For every configuration, the Geometry module delivers two shapes, one for the simulation at cruise flight and a second with a wing-aileron deflected by 10 deg. upward for the structural sizing.

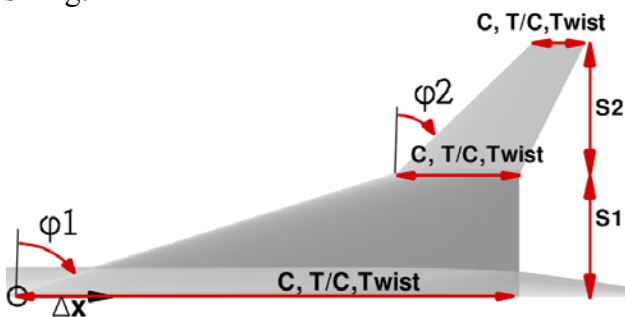


Fig. 3. Design Variables of a Generic Wing Geometry

The internal shape of the wing box is generated for facilitating FEM based structural mechanics evaluations. The structural elements include spars, ribs, covers, and stringers. Fig. 4 provides a typical example of the layout for the low sonic boom concept. In this case, the wing covers are supported by two spars and a number of ribs placed at 50-cm-span intervals. The spar and rib layout take the position of the landing-gear bays and the fuselage and engine attachment points into account. The structural topology is adapted to the changes of the wing planform/airfoils during the global-level optimization process. Different pre-defined

structural topologies are available for the different aircraft concepts.

The wing panels are stiffened using hat-type stringers for the upper-wing covers, Z-type stringers on the lower-wing covers, and blade-type stringers on spars and ribs. To reduce structural modelling turnaround times, a number of stringers are lumped together to form “numerical” stringers rather than to model each stringer individually. Also, stringers follow the wing planform taper and do not run out on the front/aft spar. The number of physical stringers that are being represented by a single numerical stringer is a design variable under the control of the structural optimization module.

The structural elements are represented by a set of structured surface meshes and are delivered to the structural optimization module for sizing of the structural elements.

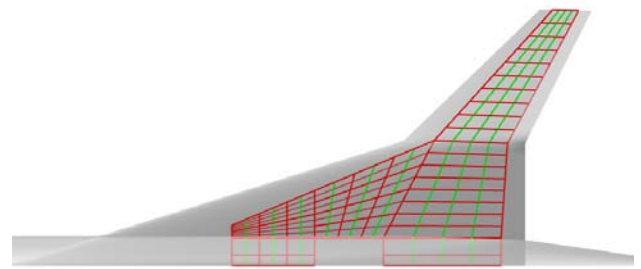


Fig. 4. Wing Internal Structural Elements

3.3 Structural optimization

The Structural Optimization module is responsible for sizing the thicknesses of the wing primary structural elements under a given representative load case. In the present study, the sizing scenario is a manoeuvre load alleviation (deflecting the wing-ailerons 10 deg symmetrically upward) at +2.5g at maximum take-off weight (MTOW) and dive Mach number and dive altitude. Under such aerodynamic loads, the wing structure experiences the maximum bending moments. An additional wing flutter analysis would lead to a more realistic sizing procedure. However, such an analysis is not available in the optimization suite and a limitation on the wing bending deformation is set instead to end up with a wing not overly susceptible to flutter. Following recommendation from a previous

study [7], the maximum bending deformation is set to 2 meters at the wing tip.

In the applications presented hereafter the aerodynamic loads are computed by the DLR flow solver FLOWer [11] in Euler mode and the structural properties of the wing are estimated by the commercial finite element code NASTRAN [12]. The thicknesses of the structural elements in the wing are also optimised by NASTRAN relying on its internal optimiser to not exceed the allowed stress level and the maximum bending deformation, so that a wing of minimal weight is obtained. Since the wing will also deform under the manoeuvre load, the aerodynamic loads have to be estimated again and the structural sizing has to be re-performed. This aero-elastic loop is iterated several times to arrive at a converged wing deflection and wing mass weight. In the present work, five couplings are performed for each configuration, this number is chosen based on practical convergence and numerical stability considerations.

3.4 CFD based aerodynamics

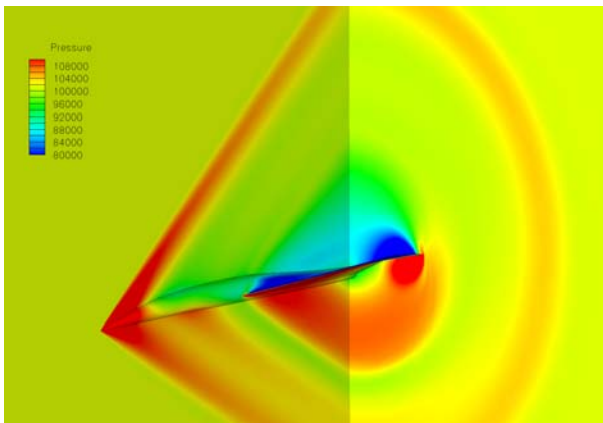


Fig. 5. Pressure Field Computed on the Low-Boom Shape Configuration ($M=1.8$)

The CFD method is used for the Structural optimization, Aerodynamic Performance and Sonic Boom Overpressure modules. The flow solver employed here is the DLR-FLOWer code running on structured meshes. The solver runs in target lift mode to automatically find the correct angle of incidence to reach the required lift coefficient. To provide the aerodynamic loads needed for the structural optimization and the performance at the start of cruise, two multi-

block structured meshes are automatically generated by the mesh generator ICEM-HEXA running in batch mode [13]. Special care was taken during the design of the mesh to capture the shocks in order to provide accurate data to the Sonic Boom Overpressure model. The resulting mesh features 12 blocks and more than 1.3 millions mesh points. The wall clock time to get a fully converged solution is about 20 minutes on 4 AMD Opteron Quad Core Processors with 1.9 GHz (Barcelona). The computed pressure field is presented in Fig. 5 for the baseline low sonic boom concept. The shock fronts are clearly visible in the symmetry plane and in a normal cut located behind the wing.

3.5 Sonic boom physics and prediction

3.5.1 The sonic boom physics

Sonic boom signals are impulsive, high magnitude sound signals felt by a static observer at ground level. Sonic booms are the result of the nonlinear propagation of shock waves through the atmosphere, down to the ground, due to the pressure disturbances generated by supersonically traveling aircraft, see Fig. 6. During their propagation in the atmosphere, the shape of the time signal associated to these pressure perturbations evolves under the competing non-linear and dissipative effects. The non-linear effects tend to generate steep shocks through coalescence of successive pressure perturbations. On the contrary, the different dissipative effects, dominated by molecular relaxation phenomena, tend to thicken and dissipate shocks.

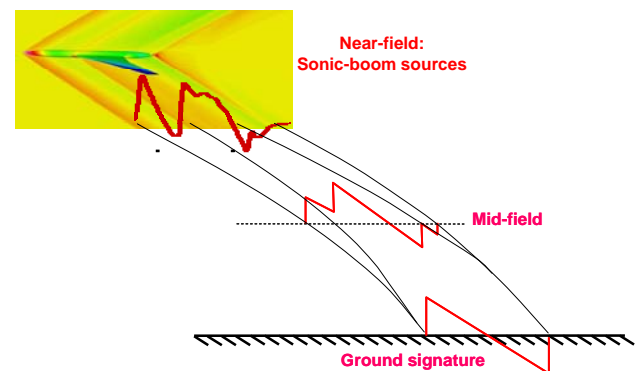


Fig. 6. Sonic Boom Physics.

3.5.2 Numerical evaluation of the ground-propagated sonic boom

Simulating the sonic boom is an intricate task involving complex physical phenomena and very different scales. An accurate modeling of the sonic boom first requires an adequate prediction of its sources, the aerodynamic pressure disturbances generated by the aircraft in its close vicinity. In this region, the aerodynamic flow is governed by the non-linear Euler equations and includes three-dimensional features with scales proportional to the aircraft length. Therefore CFD methods are perfectly suited and necessary to predict these near-field aerodynamic perturbations giving birth to the sonic boom. Because the prediction of the sonic boom requires propagating the pressure signal from the aircraft down to the ground over tens of kilometers, i.e. several hundreds of the aircraft length, conventional CFD methods are inadequate to perform this long distance propagation. They would require a tremendous number of mesh points and would eventually fail to capture important effect occurring during the propagation (such as the molecular relaxation which is an important dissipative phenomenon for sonic booms not taken into account in present CFD code models, contrary to the classical thermoviscous effects). Therefore, a specific acoustic code is necessary to carry out this long distance propagation of the sonic boom signal through the standard atmosphere which is stratified and includes temperature and density changes with altitude.

The sonic boom prediction methodology used in this work is based on a three-layer approach, as illustrated in Fig. 7. Layer 1 corresponds to the near-field aerodynamic flow prediction with CFD. Layer 3 is the atmospheric propagation of the sonic boom with an acoustic code, while layer 2 ensures a natural matching between the near-field aerodynamic data and the native inputs of the acoustic code.

Examples of the application of these methods to supersonic business jet configurations can be found in [14].

Layer 1: Near field aerodynamic calculation by CFD

First, the pressure perturbations in the close vicinity of the aircraft flying at supersonic

cruise conditions, which are the origin of the sonic boom, are calculated by solving the three-dimensional steady Euler equations. To obtain an accurate evaluation of the near-field aerodynamic pressure perturbations, specific care must be given to the quality of the CFD mesh which must have characteristics adapted to the flow physics of these perturbations traveling along flow characteristics. The computational domain of this CFD calculation typically extends between twice and four times the aircraft length around the aircraft. In the present work within the HISAC project, the CFD meshes and solutions were generated and calculated by DLR.

Layer 2: Multipole matching method

The CFD-aerodynamic pressure field is extracted on a cylinder surrounding the aircraft, aligned with the flow direction, whose radius is a user-specified parameter varying between one half to one body length. The pressure perturbations on this cylinder are then post-processed using the multipole decomposition method originally introduced by Plotkin and Page [15, 16] and applied by Salah El Din [17]. This decomposition method proceeds through a development of the near field pressure signature on the cylinder according to the azimuth variable θ . Thereby, it allows to rebuild a Whitham function equivalent, at long distance, to the pressure perturbation generated by the aircraft, while cumulating the diffraction effects associated to the non-axisymmetrical near-field flow. The ground signature computed from this equivalent rebuilt Whitham function is observed to converge much faster with the matching distance between the CFD and the acoustic theory (i.e. the radius of the cylinder) than the ground signature from a direct CFD/acoustic would match. This justifies the use of this second layer which, further to providing a theoretically correct near-field/far-field match, greatly reduces the CFD grid size needed for the near field computation, saving significant computing time.

This method calculates the cumulated effects of diffraction occurring during the propagation of the sonic boom signal from its source in the near field to the far field. These

effects are then transferred to the cylinder of radius R where the pressure disturbances are extracted in the near field. For that, the equivalent Whitham function of the pressure signal is decomposed (see [17] and [14] for more details):

1. at a constant radius value R , using Fourier series along θ (see eq. 1 below), the azimuthal direction;
2. and according to series of multipole functions (see eq. 2 and 3), which are functions of radius R and longitudinal distance τ .

The first decomposition provides the coefficients of the different Fourier modes from the aerodynamic pressures on the cylinder of radius R (eq. 4 and 5). The second decomposition involves integrals along the longitudinal direction of complex functions A_n which are calculated by identification between the two decompositions. The matching Whitham function F_{rac} is finally obtained by having $R \rightarrow \infty$ in the second decomposition (eq. 6 and 7).

$$F(\tau, R, \theta) = \sum_{n=0}^{\infty} F_n(\tau, R) \cos n\theta \quad (1)$$

$$F(\tau, R, \theta) = \frac{1}{2\pi} \sum_{n=0}^{\infty} \cos n\theta \int_0^{\tau} \frac{A_n(\xi) G_n(\tau - \xi, R)}{\sqrt{\tau - \xi}} d\xi \quad (2)$$

with

$$G_n(\tau, R) = \frac{ch \left[n \operatorname{arg} ch \left(1 + \frac{\tau}{\beta R} \right) \right]}{\sqrt{1 + \frac{\tau}{2\beta R}}} \quad (3)$$

$$F_0(\tau, R) = \sqrt{\frac{\beta R}{2}} \frac{1}{\pi} \int_0^{\pi} C_p(\tau, \theta, R) d\theta \quad (4)$$

$$F_n(\tau, R) = \sqrt{\frac{\beta R}{2}} \frac{1}{\pi} \int_0^{\pi} C_p(\tau, \theta, R) \cos n\theta d\theta \quad (5)$$

$$F_{rac}(\tau, \theta) = \sum_{n=0}^{\infty} F_n(\tau, \infty) \cos n\theta \quad (6)$$

with

$$F_n(\tau, \infty) = \frac{1}{2\pi} \int_0^{\tau} \frac{A_n(\xi)}{\sqrt{\tau - \xi}} d\xi \quad (7)$$

τ being the distance :

$$\tau = x - \beta R \text{ and } \beta = \sqrt{M^2 - 1} .$$

Layer 3: Atmospheric propagation method

Finally, the ground signature is computed by propagating the near-field aerodynamic pressure perturbations matched by the multipole decomposition method (layer 2) using the non-linear acoustic propagation code, *TRAPS* [18]. *TRAPS* is a dedicated sonic boom propagation code based on the inviscid non-linear acoustic theory. It uses a ray-tracing approach to account for refraction phenomena occurring during the propagation through a stratified atmosphere with vertical temperature and density gradients and to evaluate the extent of the “primary carpet”, i.e. the width of the corridor underneath the aircraft trajectory directly affected by the sonic boom. Along each acoustic ray, the Whitham theory (first order correction to the linear supersonic theory) is used to predict the evolution of the shape of the sonic boom pressure signal. For the propagation along the acoustic rays, the *TRAPS* code implements an inviscid non-linear one dimensional propagation equation (1D Euler equation) and therefore does not take into account any dissipation phenomena (neither thermoviscous nor molecular relaxation). This assumption does not allow for an evaluation of the rise time which is the time the pressure needs to jump from the value just before to the value just after the shock. However it does allow an accurate evaluation of the level of overpressure of each of this shock. Corrections have been implemented to include a rise time for each of the shocks composing the signal but due to stability problem of the process it was not activated during the optimizations.

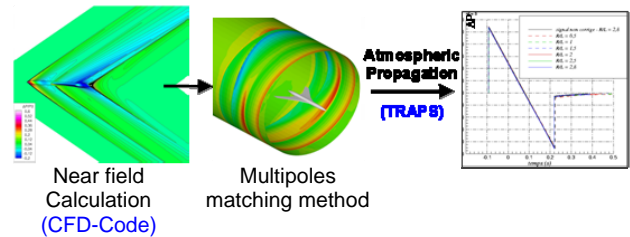


Fig. 7. Three-Layer Sonic Boom Prediction Methodology

3.5.3 Criteria for sonic boom minimization

Based on NASA studies, the most relevant metric for a single event sonic boom loudness is either the Sound Exposure Level with standard A-weighting (A-SEL) or the Perceived Level (Stevens Mark VII procedure) (PL). However, these metrics are not easy to relate directly to ground pressure signatures because they integrate the human ear response as a function of frequency, and are strongly influenced by the rise time of the shocks. During the HiSAC project, a simpler metric for sonic boom minimization was suggested which is based on the maximum magnitude of every shock that appears along the signature and not only the first shock magnitude, or the maximum overpressure. The proposed target shock magnitude was 15Pa.

A dedicated sonic boom analyser has been developed by Onera that gives the maximum magnitude of all shocks in the sonic boom signature at the ground. If successive shocks occur within a short period of time, typically within 7 ms, they are then recombined into a unique shock with a magnitude equal to the sum of all successive pressure jumps.

3.6 Optimization strategy

The objective of the work is to obtain the trends between the maximum take-off weight, the mission range and the sonic boom metric for each configuration. Additionally to these objectives, two constraints are applied to guarantee that the aircraft can be trimmed at cruise flight and is statically stable during approach. From previous studies, it was observed that the final configuration depends on the initial configuration since the design space presents numerous local minima. Furthermore the sonic boom metric as defined above can not be continuous in the design space. For these reasons, a genetic algorithm is preferred and the Adaptive Range Multi-Objective Genetic Algorithm (ARMOGA) available in modeFRONTIER [19] is selected.

The average turn around time for the evaluation of a single configuration, that involves 5 CFD-CSM couplings and a flow computation in cruise condition for performance

and sonic boom prediction is about 1 hour wall clock time. In order to speed up the optimization process, up to 10 evaluations are performed simultaneously.

4 Optimization of the low boom concept

For the optimization of the low sonic boom concept, the goals are to minimize the MTOW and the sonic boom impact on the ground for a given target range. The definition of the range considered in the study is the distance travelled at landing at the scheduled destination with enough fuel reserves for a diversion and loitering flight. For the low boom concept, the target range is set to 4600nm with a cruise Mach number of 1.8 and an initial cruise altitude of 53,000 feet.

For this multi-objective optimization, 13 geometrical design parameters are used to change the planform, twist and shape of the wing, see section 3.2. For the low boom concept, the inner- and outer-wing dihedrals, favorable for sonic boom mitigation, are also used as design parameters.

The optimization was initialized through a design of experiment (DOE) made up of the baseline configuration and a Latin Square method with 7 levels. The resulting DOE contains 50 entries and is then used as the initial population for the multi-objective genetic algorithm ARMOGA. To speed the optimization process, up to 10 evaluations are conducted simultaneously. It takes about 20 days wall clock time to perform 100 generations.

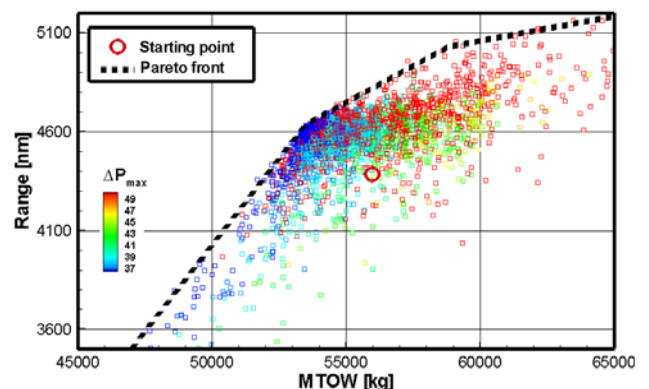


Fig. 8. Range, MTOW and Shock Magnitude (in color) for all evaluated configurations.

Fig. 8 presents all successful evaluations as a square in a MTOW versus the mission range diagram where the color of the squares indicates the shock magnitude. By nature the optimizer spreads the individuals throughout the whole design space but about 2000 evaluations are concentrated around the target range of 4600nm, which implies that the optimization process is converged. From the figure, an optimal Pareto front between MTOW and Range clearly exists and can be divided into three segments: for optimal aircrafts with a MTOW lower than 53.5t, a 1t increase in MTOW allows an extension of the range by 174nm; above this MTOW, the ratio decreases to 75nm per ton and finally becomes negligible above 58.6t MTOW. For the sonic boom metric however, no clear trend is visible. The shock magnitude tends to be related to the MTOW, but some configurations with low sonic boom could be found up to 60t MTOW.

In order to identify the reason for the range and weight improvement, the lift to drag ratio in cruise (L/D) versus the wing group weight (WGW) is plotted, see Fig. 9. For more clarity, only configurations with a mission range from 4500nm to 4700nm are plotted. Here also a Pareto front between MTOW and L/D clearly exists. In the same plot the color of the squares is related to the MTOW and we found out that the lowest MTOW configurations are the points located on the Pareto front.

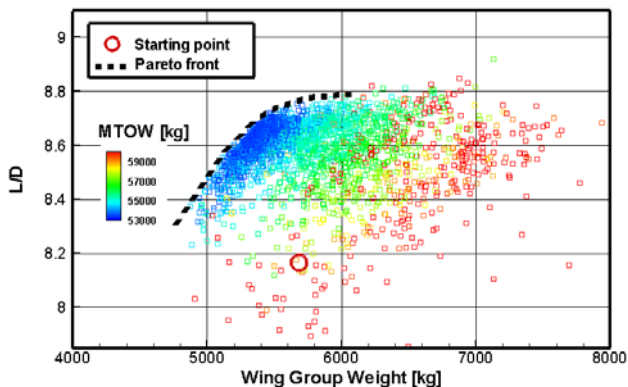


Fig. 9. L/D vs. WGW for configurations with a mission range between 4500nm and 4700nm.

With such a databank, it is pretty easy to select a geometry that presents good performance. Design 7194 has been selected because it achieved the target mission range

(4591nm) with a minimum MTOW (53.4t) and a reduced maximum pressure jump in the sonic boom signature (37.9Pa). Compared to the baseline design, this optimized configuration has a range improvement of 200nm, while decreasing the MTOW of 2.6t - mainly due to a 300kg decrease in the WGW and an L/D improvement from 8.2 to 8.7 - and a 6.6Pa reduction in the sonic boom signature.

The new shape is characterized by an increase of the outer wing sweep of 8 deg., a massive reduction of the inner dihedral (-10 deg.) compensated by an increase of the outer wing dihedral (+7 deg.), as shown in the lower half of Fig. 10 and Fig. 11 respectively. The pressure distribution at cruise for the baseline and optimized configurations are compared in Fig. 10. The increase in the outer wing sweep leads to lower drag in cruise flight.

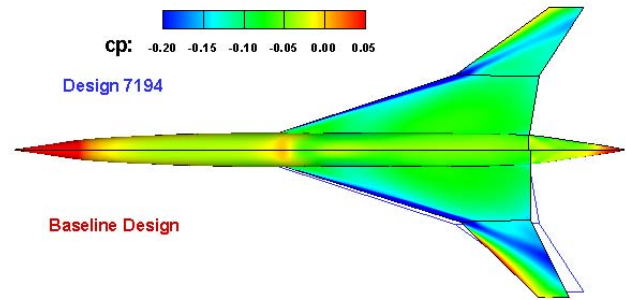


Fig. 10. Pressure Distribution for the baseline and optimized low boom sonic concepts (M=1.8).

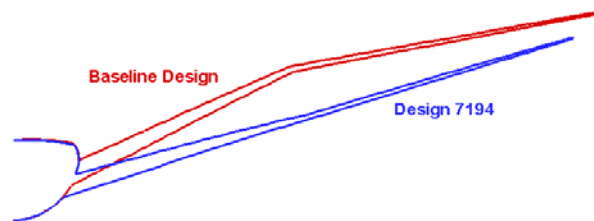


Fig. 11. Dihedral of the baseline and Design wings.

As expected, the sonic boom signature is modified due to the dihedral, but it still presents the classical sonic boom N shape, see Fig. 12. The decrease of the shock strength has been mainly obtained at the tail of the signature, with an improvement of about 6.6Pa of the minimum pressure level. In contrast, the maximum pressure level increases by 3.6Pa, but since the front is divided into 2 main shocks, one at the origin and a second 7.3 ms later each shock is considered as separated. Under the assumption

that the shock strength is the sum of each pressure jump within 7ms, the optimized configuration presents then an increase of pressure of 0.4Pa and 0.5Pa for the first and second shock respectively.

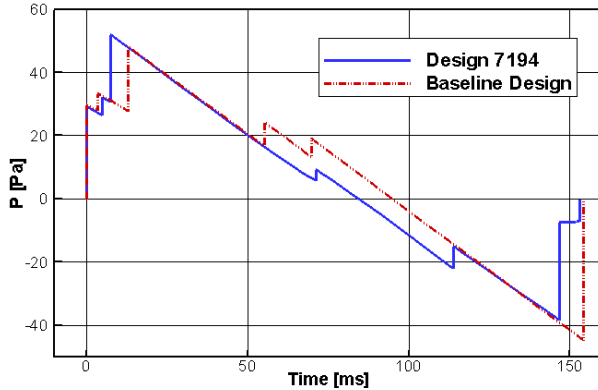


Fig. 12. Sonic Boom Signature for the Baseline and Best Concepts (Design 7194).

From the optimization point of view, the process succeeded to find an optimal configuration meeting the target range of 4600nm, while decreasing the MTOW by 2.6t (-4.7%) and the maximum pressure jump by 6.6Pa (-15.6%) compared to the baseline configuration. However, the improvement of the sonic boom criteria is merely relying on the hypothesis that 2 shocks will not recombine to a single stronger shock if they are separated by more than 7ms. It is also worth to mention that the engine nacelles and tail planes are neglected during the sonic boom evaluation and probably have an impact on the shock signature, in particular at the end of the *N* wave. We thus decided to search in the database for a configuration with a low maximum overpressure without too much penalty on the mission range. Design 1525 presents a sonic boom signature characterized by a front shock split into 3 well separated small shocks with a maximum overpressure of 38Pa, see upper part of Fig. 13. To attain such good sonic boom signature, the optimal shape enforced the characteristics of the baseline concept, with a high inner-wing dihedral and span, see lower part of Fig. 13. However, the resulting aircraft has a quite high MTOW (58,3t) for a limited range (3910 nm): the increase of MTOW is due to a high WGW, +23% higher than the baseline configuration.

In conclusion, the MDO process permits the quantification of the trade-off between the mission range, the MTOW and the sonic boom and highlights the conflicting criteria required for optimal configurations. For the sonic boom metric, no clear trend is observed, save for the need of a high wing dihedral and reduced weight. It was also found that a decrease of the wing dihedral angle combined with an increase of the outer sweep angle offers great potential for increasing the mission range, reducing the MTOW without penalty on the sonic boom metric. Finally, the target shock magnitude of 15Pa seems unachievable through merely a wing shape modification, and a careful design of the fuselage nose, like a round nose or a quiet spike, is mandatory.

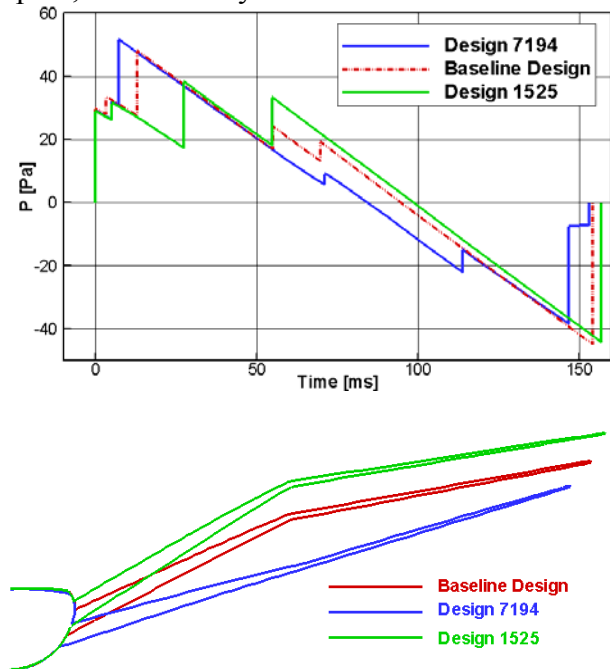


Fig. 13. Sonic Boom Signature (Top) and Dihedral (Bottom) for the Baseline, Best and Lowest Overpressure Concepts (Design 1525).

5 Optimization of the long range concept

The target range for the long range concept is 5000 nm in order to be able to perform missions between North America and Europe or the Middle East and to cross the Pacific Ocean with a single refuelling stop. The baseline configuration is a simple fuselage without area ruling, with a mission range of 4800nm at 58t MTOW and a maximum shock magnitude of 80.6 Pa. Based on previous analysis, a realistic

transition location is assumed to be at 50% chord.

For this optimization, 12 geometrical design parameters are used and change the wing planform, the twist and thickness of the wing at 3 sections. Here, the wing dihedral is not allowed to change and the inner- and outer-wing sweeps are identical to avoid a leading edge crank. The same MDO procedure as before is applied and after 40 generations, the process is stopped.

Fig. 14 presents the MTOW vs. the mission range for all evaluated configurations and the squares are colored according to the maximal pressure jump in the sonic boom signature. One can observe a simple Pareto front between mission range and MTOW.

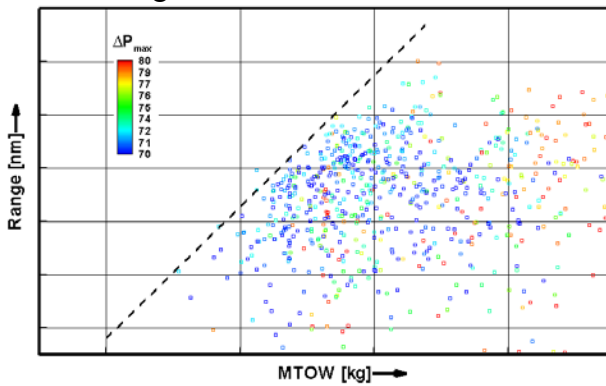


Fig. 14. Range, MTOW and maximum Shock Magnitude (color) for all evaluated configurations.

Once the optimization completed it was observed that the aileron size was set too large for this optimization (66% of the span instead of 33% as the original configuration): the resulting wing sizing procedure was then very “conservative” resulting in a much too heavy wing, an underestimation of the fuel weight and a reduction of the mission range: the trend between MTOW and range can not be quantified exactly here. However, since all configurations were computed with the same procedure, it is assumed that the trade-off between MTOW and mission range is not affected too much by the improper aileron setting. Due to time constraints, it was not possible to redo the multi-disciplinary optimization and it was decided to analyze the database in detail and to post-process several configurations with the correct aileron size. To avoid any confusion, all data presented in this

paper - except for Fig. 14 - are obtained with the correct aileron size (33% of span).

An optimal configuration presenting a high L/D and a low shock magnitude was selected from the database and was re-computed with the correct aileron size and with an adapted MTOW to match the target mission range of 5000nm. This configuration, called Design 1486, presents excellent performance compared to the baseline configuration: the mission range is increased by 200nm (Range=5007 nm) while decreasing the MTOW by -1.5t (MTOW=56.5t) and the maximum shock magnitude by -10 Pa ($\Delta p_{max}=70.3$). The increase of the mission range is due to a +0.8 increase in L/D (L/D=8.5) but penalized by a +1.1t increase in wing group weight. The resulting wing shape and pressure distribution is given in Fig. 15. The new design is characterized by a crank at the trailing edge and an increase in the wing sweep (+7deg.) and in wing twist. In fact, the new twist law permits to decrease the angle of attack by -3deg at same lift coefficient which helps to lower the drag and shock magnitude, see Fig. 16. However, it can be observed that the reduced sonic boom signature still presents a strong N wave shape.

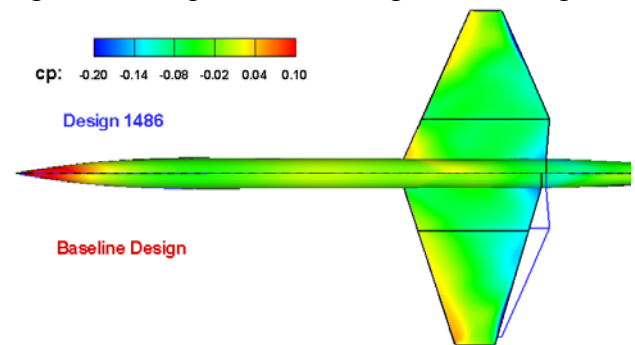


Fig. 15. Pressure Distribution for the baseline and optimized long range concepts (M=1.6).

In an attempt to get a more aggressive improvement of the shock signature, a single disciplinary optimization is finally performed with 11 additional design variables for the fuselage shape. The objective focuses solely on the minimization of the shock magnitude. To lower the turn around time, only the sonic-boom module is used and the CFD computations, performed at constant lift coefficient, are conducted on a coarse mesh. To ensure a global search, a genetic algorithm (differential evolution [20]) is employed with a small

population size computed in parallel on a cluster. After 2 days wall clock time, the process converges to the optimal configuration called DE4937. To present consistent results, the optimal configuration is then evaluated using the (full) multi-disciplinary suite described previously. The maximum shock magnitude is now reduced to 49Pa, which represent a 20Pa decrease compared to the previous optimization. The resulting sonic boom signature is plotted in green in Fig. 16: the new optimal sonic boom signature is characterized by a decrease of the shock magnitude mainly at the aft of the signal, but the *N* form still exist with limited change at the front part.

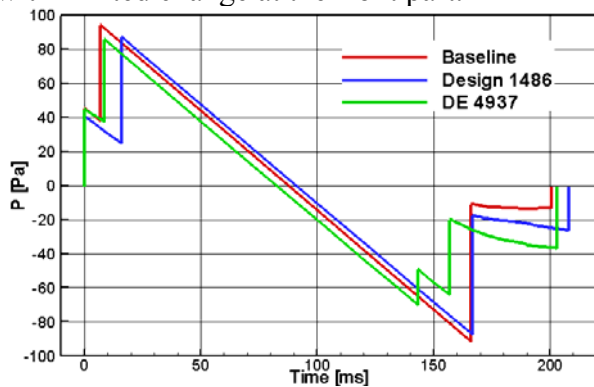


Fig. 16. Sonic Boom Signature for the Baseline, Best Long Range (Design 1486) and Long Range Concept with Lowest Shock Magnitude (DE 4937).

Fig. 17 presents the optimized shapes and both wings are characterized by a crank at the trailing edge. However, configuration DE4937 has a lower sweep angle and a fuselage shape presenting reduced radius at the wing leading and trailing edges: the fuselage shape is here adapted for minimum sonic boom signature but does not follow necessary the classical low drag area ruling.

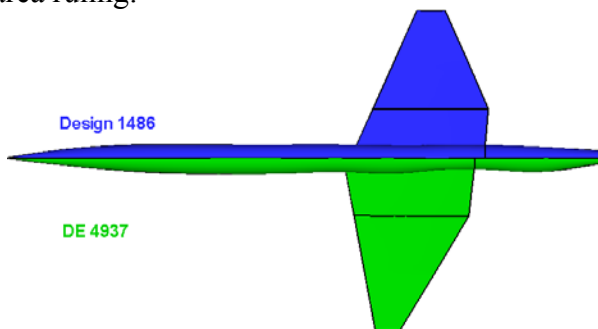


Fig. 17. Shapes of the Best Long Range Concept (Blue) and of the Long Range Concept with Lowest Shock Magnitude (Green)

The application of the multi-disciplinary suite confirms that the new configuration has poor performance with a very low *L/D* (only 5.8), a high *WGW* (9t) and only 2790nm range mission for a 58t *MTOW*.

6 Conclusion

During the HiSAC project, a multi-disciplinary optimization framework based on a multi-fidelity approach and including environmental aspect was developed for small size supersonic aircraft and successfully applied to the multi-objective optimization of a low sonic boom and a long range concept aircraft. Such an MDO chain permits the capturing of the trade-offs between mission range and maximum take-off weight, low sonic boom signature and efficient aerodynamic performance.

The study made clear that the low sonic boom concept can produce a low boom signature while improving the mission range up to 4600nm by setting appropriate wing dihedral and sweep. A more drastic reduction of the sonic boom signature would also be possible but at the cost of a massive reduction of the mission range and an increase of the *MTOW*.

The long range concept can achieve 5000nm mission range, but the resulting sonic boom still presents high shock magnitudes notably at the front side, which appears difficult to be further reduced with the current parametrization. A dedicated parametrization of the nose should help to obtain a further decrease.

Finally, the sonic boom evaluation relies on a simplified geometry and the impact of rear engine and tail planes have not been quantified here and should be investigated in the future. It would also be of interest to implement additional environmental aspects like emissions and take-off noise to explore other trade-offs between aircraft performance and the environmental impact.

References

- [1] Deremaux, Y, "Why a small size supersonic transport aircraft? Objectives and trade-offs", HISAC 2009 conference, Paris, June 2009.
- [2] Herrmann, U., "CISAP: Cruise Speed Impact on Supersonic Aircraft Planform – a Project Overview", *AIAA 2004-4539*, 10th AIAA/ISSMO Multidisciplinary Analysis and Optimization Conference, Albany, New York, 2004.
- [3] Laban, M., "Multi-Disciplinary Analysis and Optimization of Supersonic Transport Aircraft Wing Planforms", *AIAA 2004-4542*, 10th AIAA/ISSMO Multidisciplinary Analysis and Optimization Conference, Albany, New York, 2004.
- [4] Carrier, G., "Multi-Disciplinary Optimisation of a Supersonic Transport Aircraft Wing Planform." European Congress on Computational Methods in Applied Sciences and Engineering, ECCOMAS, 24-28 July 2004.
- [5] Parnis, P., "High Speed Aircraft (HISAC) - A European "Integrated Project", II International Scientific and Technical Conference, Moscow, Russia, Dec. 2005
- [6] Laban, M., Herrmann, U., "Multi-Disciplinary Analysis and Optimisation Applied to Supersonic Aircraft; Part 1: Analysis Tools", *AIAA 2007-1857*, 3rd AIAA Multidisciplinary Design Optimization Specialist Conference, Honolulu, Hawaii, April 2007.
- [7] Herrmann, U., Laban, M., "Multi-Disciplinary Analysis and Optimisation Applied to Supersonic Aircraft; Part 2: Application & Results", *AIAA 2007-1857*, 3rd AIAA Multidisciplinary Design Optimization Specialist Conference, Honolulu, Hawaii, April 2007.
- [8] P. Arendsen. Final Report of the Garteur Action Group SM AG-21 on "Multi-Disciplinary Wing Optimisation". NLR-TR-2001-557, 2001.
- [9] E. Kessler, M. Laban, W.J. Vankan. Consistent Models for Integrated Multi-Disciplinary Aircraft Wing Design". International Conference on Non-Linear Problems in Aerospace and Aeronautics, 2006.
- [10] M. Laban. A Computational Design Engine for Multi-Disciplinary Optimisation with Application to a Blended Wing Body Configuration. 9th AIAA/ASSMO Multidisciplinary Analysis and Optimization Conference, Atlanta 2002.
- [11] Kroll, N., C.-C. Rossow, K. Becker and F. Thiele, "MEGAFLOW – A Numerical Flow Simulation System", *Aerospace Science Technology*, Vol. 4, pp. 223-237, 2000.
- [12] MSC.NASTRAN 2001, "Quick Reference Guide", MSC Software Corporation, USA, 2002, www.mscsoftware.com.
- [13] Ansys, Inc, ICEM-CFD, <http://www.icemcfd.com>
- [14] R. Grenon, M.-C. Le Pape, F. Montigny-Rannou ; "Évaluation de méthodes de raccordement évoluées entre l'aérodynamique et la propagation acoustique pour la prévision du bang sonique" ; ONERA RT 2/10295 DSNA, Mars 2006.
- [15] Plotkin, K. J., and Maglieri, D. J., "Sonic Boom Research: History and Future"; *AIAA Paper 2003-3575*, 2003.
- [16] K. Plotkin, J. Page; "Extrapolation of sonic boom signatures from CFD solution" ; *AIAA 2002-0922* ;
- [17] I. Salah el Din; "Contribution à l'optimisation de la forme aérodynamique d'un avion de transport supersonique en vue de la réduction du bang" ; Thèse de doctorat, Université de Poitiers, Décembre 2004.
- [18] A.D. Taylor ; "The TRAPS sonic boom program" ; NOAA Technical memorandum ERL-ARL-87, July 1980 ;
- [19] Esteco, modeFRONTIER V4, <http://www.esteco.com>
- [20] Storn R, Price K. Differential Evolution - a simple and efficient adaptive scheme for global optimization over continuous spaces. *Technical Report*, International Computer Science Institute, TR-95-012, Berkley, 1995.

Copyright Statement

The authors confirm that they, and/or their company or organization, hold copyright on all of the original material included in this paper. The authors also confirm that they have obtained permission, from the copyright holder of any third party material included in this paper, to publish it as part of their paper. The authors confirm that they give permission, or have obtained permission from the copyright holder of this paper, for the publication and distribution of this paper as part of the ICAS2010 proceedings or as individual off-prints from the proceedings.